# Molecular dynamics simulation of the capillary leveling of a glass-forming liquid

I. Tanis, K Karatasos, Thomas Salez

# Molecular dynamics simulation of the capillary leveling of a glass-forming liquid

I. Tanis[1*], K. Karatasos[2,3], T. Salez[4,5]

[1]Laboratoire de Physico-Chimie Théorique, UMR CNRS Gulliver 7083, ESPCI Paris, PSL Research University, 75005 Paris, France
[2]Laboratory of Physical Chemistry, Department of Chemical Engineering, Aristotle University of Thessaloniki, 54124, Thessaloniki
[3] Institute of Electronic Structure and Laser, Foundation for Research and Technology - Hellas, P. O. Box 1527, 711 10 Heraklion Crete, Greece
[4]Univ. Bordeaux, CNRS,LOMA,UMR 5798, F-33405, Talence, France
[5]Global Station for Soft Matter, Global Institution for Collaborative Research and Education, Hokkaido University, Sapporo, Hokkaido 060-0808, Japan

*tanis.ioannis@gmail.com

**Abstract.** We study the evolution of square-wave patterns at the free surface of a glass-forming binary Lennard-Jones mixture over a wide temperature range, by means of molecular dynamics simulations. Particular emphasis is given on the surface diffusion which is found to be considerably faster with respect to the bulk, below the glass-transition temperature, in agreement with experimental and simulation data for organic glasses. Specifically, the pattern's amplitude is recorded as a function of time and the associated decay rate is extracted. Layer-resolved dynamic analysis further reveals that surface diffusion governs the relaxation below the glass transition temperature. Diffusion coefficients of the surface particles are larger than those in the bulk by a factor that reaches $10^4$ at the lowest temperature studied. These deviations grow upon cooling.

## I. Introduction

Thin films and their free interfaces are used in a variety of applications such as

catalysis[1], fast crystal growth[2, 3] and the formation of low-energy glasses[4, 5]. Apart from their applications in industry and technology, molecular mobility and relaxation at surfaces and interfaces have been recently a subject of growing interest for fundamental research. To this end, several experimental approaches have been used to probe the surface evolution and mobility of thin films[6-10]. More specifically, an efficient way to gain insight into the surface mass transport and the associated dynamics, is to deposit nanoparticles on the film surface and subsequently to monitor the host material's response[9, 11]. Another powerful and versatile technique widely utilized for the determination of the surface-diffusion coefficient $D_s$, characterizing the in-plane translation of molecules at the film surface, is the capillary-driven leveling of surface-gratings [6, 9, 12-14]. Several studies suggest that the mechanism governing the relaxation of these gratings is temperature and material dependent[12, 15]. More specifically, recent works on glass-forming molecular liquids reported a transition from bulk viscous flow at temperatures higher than the glass-transition temperature $T_g$, to surface diffusion below $T_g$[13, 16]. Analogous studies in polymeric liquids revealed that bulk viscous flow was the only mechanism governing the surface decay, even at the highest viscosities studied[14, 17, 18]. According to Mullin's pioneering work[19], the different mechanisms that could flatten the surface pattern (surface and bulk diffusions, evaporation-condensation, bulk viscous flow) can be distinguished by determining the decay rate dependence on spatial frequency. This method has been applied in crystalline metals[20], amorphous silica[21] and molecular glasses[22].

Measurements of diffusion coefficients of surface particles report values considerably higher than the respective bulk coefficients at the glass-transition temperature[12, 13]. Furthermore, large variations in surface diffusion coefficients among different molecular glass formers bearing a similar bulk mobility were linked to the strength of the intermolecular forces[23].

Further insight into glass-forming systems has been provided by molecular simulations. Several studies have addressed the factors that govern dynamical heterogeneity and spatial correlations in the bulk[24-28]. Furthermore, other works addressing systems under confinement have managed to elucidate the effects of confinement by rough or smooth walls on the liquid dynamics and to extract associated lengthscales[28-33]. Extensive simulation studies have also been conducted on ultrastable vapor-deposited glasses[4, 34, 35]. However, to our knowledge, a small

number of simulation studies probing the surface mobility in molecular glass formers have been reported so far.

Surface-diffusion-mediated decay of two-dimensional nanostructures has been recently studied by a combined analytical and kinetic Monte-Carlo approach[36], whereas Kayhani *et al*. performed molecular dynamics simulations to examine the coalescence of platinum nanoclusters[37]. Concerning simulation work on surface mobility of molecular glass formers, Hoang et al. performed molecular dynamics (MD) studies on freestanding monatomic glass-forming liquids[38]. The study of Akbari *et al*. addressed the effects of substrate in kinetic and thermodynamic properties of a binary Lennard-Jones (LJ) liquid[39], whereas Malshe and co-workers extracted surface-diffusion coefficients by the aid of the grating-decay approach[40] in freestanding films of the aforementioned liquid type. Results were consistent with data obtained from the mean-squared displacements of the liquid particles.

The aim of the present work is to provide additional insight into the surface mobility of a glass forming liquid by means of MD simulations. Similarly to a recent work where we probed the viscoelastic behaviour of nonentangled polymer films above $T_g$ through the capillary leveling of a square-wave surface pattern[41], we examine the evolution of a similar surface topography atop a binary LJ mixture supported by an attractive substrate. This study is carried out over a wide temperature range, sampling both the glassy and liquid states of the film. The associated decay rates are extracted whereas surface and bulk mobilities are examined and compared with existing data.

## II. Simulation details

We examine a binary mixture of 80% A and 20% B particles that interact via a LJ potential $V_{\alpha\beta} = 4\epsilon_{\alpha\beta}\left[\left(\sigma_{\alpha\beta}/r\right)^{12} - \left(\sigma_{\alpha\beta}/r\right)^{6}\right], (\alpha, \beta \in \{A, B\})$. The Van der Waals parameters were chosen as $\epsilon_{AA} = 1.0, \sigma_{AA} = 1.0, \epsilon_{AB} = 1.5,\ \sigma_{AB} = 0.8, \epsilon_{BB} = 0.5, \sigma_{BB} = 0.88$. The potential was truncated at a cut-off radius $r_c = 2.5\sigma_{AB}$. The number of particles of type A and B is 2938 and 734, respectively. The binary mixture interacting with this parameter set corresponds to the Kob-Andersen liquid model which is not prone to crystallization or to phase separation; it is extensively utilized in studies of glass-forming liquids[42, 43]. The liquid film is supported by a strongly attractive substrate whose atoms (henceforth designated by the type S) are located on

the sites of an hexagonal lattice and are kept fixed to their lattice positions. The substrate particles have radius $\sigma_S = 2.41$ and they attract A and B atoms with the following energy magnitudes[44]: $\epsilon_{AS} = 4.425$ and $\epsilon_{BS} = 3.129$. The length of the cubic box is 16.56 $\sigma_{AA}$ in the lateral directions *x* and *y*, and 441.17 $\sigma_{AA}$ in the *z* direction. The value of the latter is chosen large enough to avoid interaction of the particles with periodic images of the substrate. All quantities are reported in LJ units, *i.e.* length is measured in units of $\sigma_{AA}$, energy in units of $\epsilon_{AA}$, time in units of $\tau = (m\sigma_{AA}^2/48\epsilon_{AA})^{1/2}$ and temperature in units of $\epsilon/k_{\mathrm{B}}$ where $k_{\mathrm{B}}$ stands for the Boltzmann constant. For the case of argon, these units correspond to a length of 3.4 Å, an energy of 0.01 eV and a time of $3\times 10^{-13}$s. The binary mixture corresponds to a density (in reduced units) of $\rho = 1.2$. All simulations are performed in the canonical (NVT) ensemble using the DL_POLY code[45]. Temperature is maintained constant through the use of the Nosé-Hoover thermostat. Simulations are conducted in the temperature range $T$ = 0.20-0.525, and the duration of each run is $3\times 10^5$.

The initial configuration of the glassy film was obtained by the aid of the Aten program[46]. To create the square pattern at the free surface of the film, a flat film was initially equilibrated in the canonical ensemble at a temperature of $T$ = 0.3. Afterwards, particles were removed in a symmetrical manner in order to obtain the square pattern (see Fig.1). The lateral dimensions of the latter were $Lx$ = $Ly$ = 4.41, whereas its initial height (counted from the substrate) was $h_0$ = 15.67.

To examine the behaviour in the bulk, a configuration comprising 5076 particles was constructed at an elevated temperature, $T$ = 0.80. After removing close contacts, the system was cooled to $T$ = 0.30 by conducting runs in the isothermal-isobaric ensemble (NPT) at pressure $p$ = 0.0024. The temperature step between the isothermal runs ranged from d$T$ = 0.1 for the highest temperatures to d$T$ = 0.025 at temperatures around the bulk glass-transition temperature $T_{\mathrm{g}}$. The duration of each isothermal run ranged from $1.6\text{x}10^4$ to $3\text{x}10^5$. Defining the cooling rate as the difference between the starting temperature and the final temperature divided by the time of the quench, the cooling rate was $1.7\text{x}10^{10}$. The glass-transition temperature of the binary mixture was determined by extrapolating and intersecting the linear dependences of the low- and high-temperature specific volume curves. This yielded a value of $T_{\mathrm{g}}$ = 0.43 which compares well with data reported in the literature[40, 47, 48].

Figure 1 displays the initial configuration of the liquid model, as well as snapshots from the run at $T$ = 0.3 at times $t$ = 20000 and 233333 . The particles that evaporated at elevated temperatures were disregarded from post-analysis.

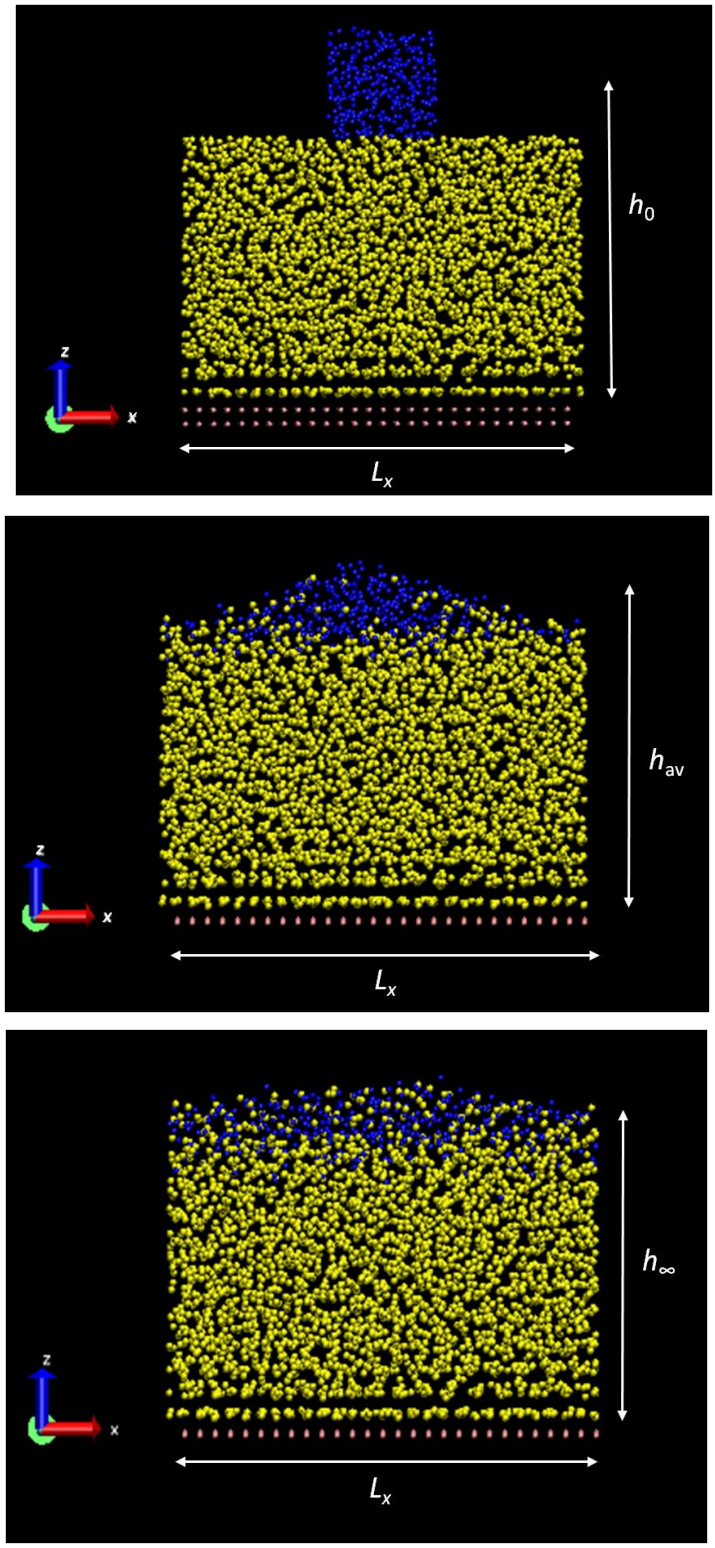

Figure 1: Top: Initial configuration of the liquid film bearing a total number of 3672 particles. Periodic boundary conditions are applied in all directions. $L_x$ stands for the *x*-dimension of the simulation box and $h_0$ is the maximum vertical height (colour code : blue = top layer, yellow = bottom layer, pink = substrate). Middle: Snapshot of the film at $t$ = 20000, where $h_{av}$ is the average height value of the top-layer particles. Bottom: Snapshot of the film at $t$ = 233333 ; $h_\infty$ is the average height of the top-layer particles in the fully leveled film.

## III. Analysis

To investigate the mobility of the liquid's molecules, it is useful to examine the probability distribution $G_s(r,t)$ of their displacements $r$, during a time $t$, *i.e.* the self-part of the van Hove space-time correlation function defined as :

$$G_s(\boldsymbol{r},t) = \frac{1}{N}\sum_{i=1}^{N}\left\langle \delta\left(\boldsymbol{r} - \left[\boldsymbol{r}_i(t) - \boldsymbol{r}_0(t)\right]\right)\right\rangle \qquad (1)$$

with $\boldsymbol{r}_i = (x_i, y_i, z_i)$ being the position of particle $i$, $N$ being the number of particles that constitute the film top layer, $\langle \ldots \rangle$ being the ensemble average over realizations and time origins and $\delta$ is the Dirac's function. In order to improve the statistics of our data, we do not distinguish between the different orientations of the vector $\boldsymbol{r}$. In Fig.2, the $r$ dependence of $4\pi r^2 G_s(r,t)$ for the molecules near the surface for two times $t$ is displayed. Also shown in the figure, are the corresponding curves for the bulk sample. The van Hove functions were evaluated at a temperature $T$ = 0.375, near the bulk $T_g$, as well as at a temperature $T$ = 0.30 which lies below the glass transition.

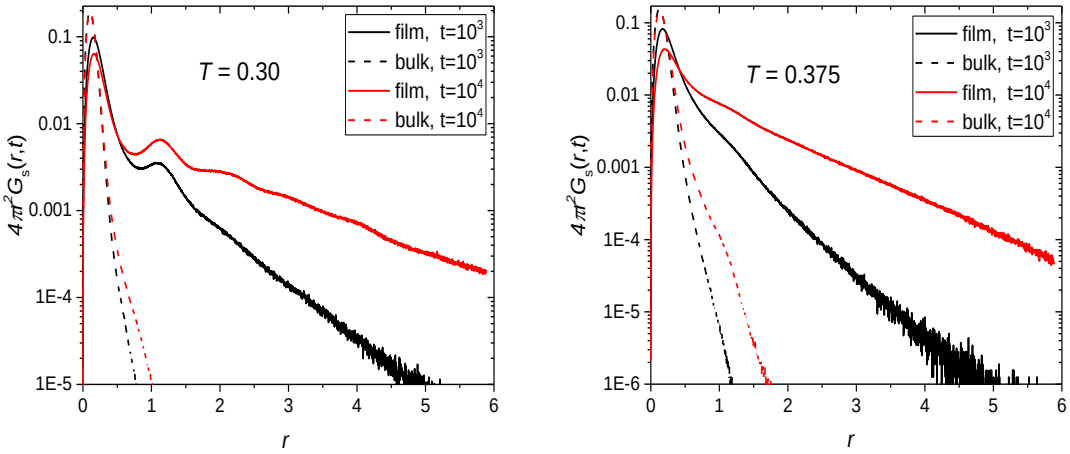


Figure 2: Self part of the generalized van Hove function (eq.1), as a function of the molecular displacement *r*, evaluated at $T$ = 0.30 (left) and $T$ = 0.375 (right). The different line colours correspond to different times and the reference for a bulk sample is provided for comparison.

A visual inspection of Fig.2 reveals that the particles from the film top layer are significantly more mobile than those residing in the bulk. Focusing on the left panel, we see that in the bulk, and at low temperature, the distribution shows a vanishing probability for *r* larger than the near-neighbour distance ($r$ = 1.0). As expected for a glassy behaviour, this implies that the particles have not managed to escape from the cages in which they were trapped initially. In contrast, the distribution for the surface particles exhibits non-negligible values up to $r \sim 5$, thus providing evidence for the enhanced mobility at the free interface of the film. As expected, the difference between surface and bulk excursions grows with time. It is also noteworthy that the deviation of the surface mobility with respect to the bulk is less pronounced at higher temperatures (see right panel), in accordance with previous findings[38, 40].

To further examine the dynamic aspects of the top-layer particles and possible deviations from a diffusive behaviour, we evaluated the non-Gaussian parameter (NGP):

$$\alpha_2(t) = \frac{5\langle \Delta r(t)^4 \rangle}{3\langle \Delta r(t)^2 \rangle^2} - 1, \qquad (2)$$

where $\Delta \boldsymbol{r} = \boldsymbol{r}(t) - \boldsymbol{r}(0)$ stands for the displacement of the top-layer particles in the time interval of duration *t*. If the NGP is nonzero, the particles are non-diffusive in the time lapse *t*. As seen in Fig.3 this is the case here at the lowest temperature shown and at intermediate time scales. Moreover, the time at which NGP exhibits a maximum denotes a characteristic lifetime of a transient cage and has been associated with the time scale at which local dynamical heterogeneities are most pronounced[25].

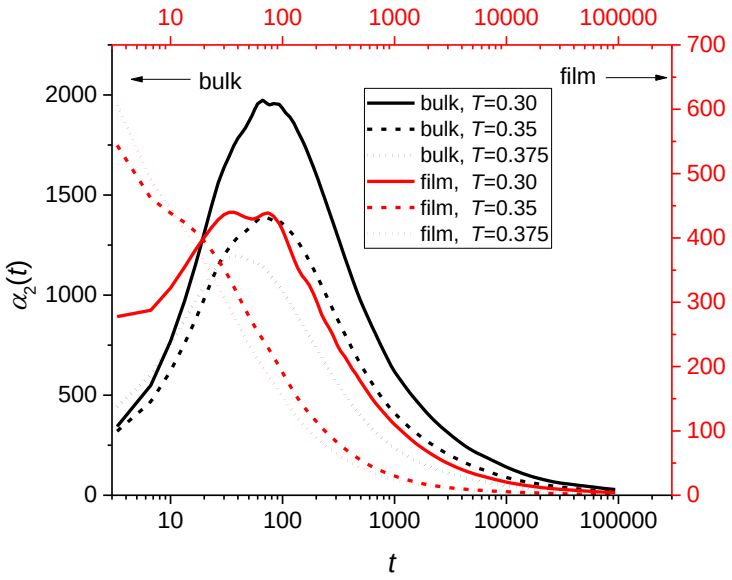


Figure 3: Non-Gaussian parameter, (eq.2), evaluated at $T$ = 0.30 and $T$ = 0.375. The reference for a bulk sample is also provided for comparison.

The aformentioned surface caging lifetime increases as temperature is decreased, which is reminiscent of the bulk behavior. However, we stress that the surface caging manifests itself only at the lowest temperature shown ($T$ = 0.30), and that rapidly after the top layer recovers an equilibrium-like diffusive behavior in sharp contrast to bulk glasses. It is also noteworthy that at very short times we do not observe the expected close-to-zero values of the NGP of the top-layer film particles, as NGP is governed by the ballistic motion of the latter. A closer inspection of the graph corresponding to the top-layer film particles at $T$ = 0.30 reveals the existence of two different maxima at $t \sim 35$ and $t \sim 80$, suggesting the existence of two different populations. We can surmise that the former peak corresponds to the particles near the top square corners/high negative curvature regions, where there are even less neighbours and more free volume. This double peak reveals a higher degree of dynamical heterogeneity at the lowest temperature and lies in accordance with the findings of

Malshe *et al.*[40]. In our case, the fine-structure separation of relaxation processes is no longer detected at $T > 0.30$, thus indicating a more homogenous surface decay process.

To examine the global consequences of the enhanced surface mobility on the film leveling, we have monitored the average height $h_{av}(t)$ of the top-layer particles. The initial value of $h_{av}$ (counted from the substrate) was $h_{av0} = 13.5$. An example of the time evolution of the rescaled amplitude, $\ln\left[\frac{h_{av}(t)-h_{\infty}}{h_{av0}-h_{\infty}}\right]$, for a temperature $T = 0.45$, is displayed in Fig.4a, where $h_{\infty} = 11.31$ is the average height of the top layer in the fully leveled film. It should be noted here that the simulation runs at elevated temperatures were characterized by a very rapid relaxation of the square pattern and, concurrently, a significant number of particles that evaporated before the film full leveling. To avoid issues arising from poor data statistics, a value for $h_{\infty}$ higher than that predicted from volume conservation, was chosen. For consistency, this value was chosen at all temperatures studied. As can be inferred from Fig.4a, the temporal decay is exponential. Figure 4b displays the associated decay constant as a function of temperature, across the glass transition. We note that the minimum temperature at which full leveling of the square pattern was observed within the total simulation time, was $T = 0.30$.

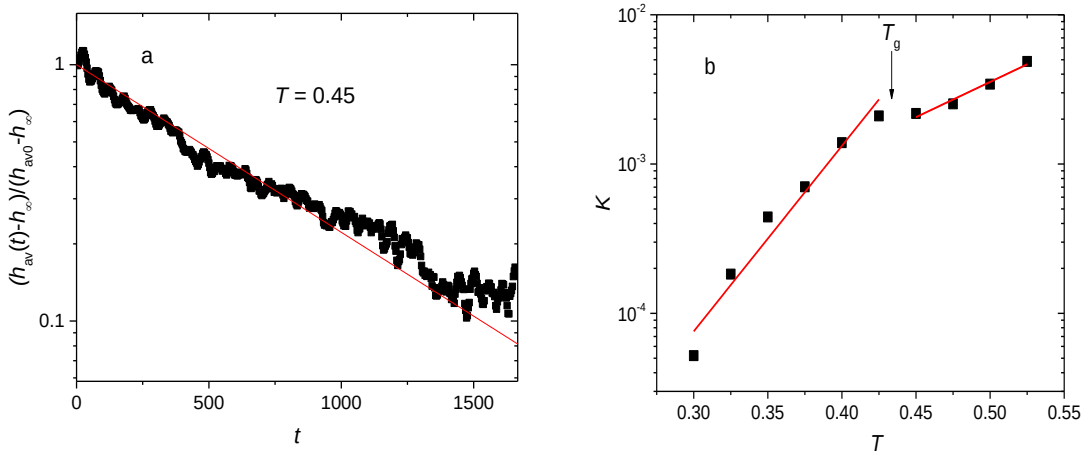


Figure 4: a) Time evolution of the rescaled pattern amplitude at $T = 0.45$. The red line is an affine fit. b) Decay constant $K$ as a function of temperature. Error bars in $K$ are on the order of $10^{-6}$.

Examining Fig.4b, it appears that a mechanism distinct from the one above $T_g$ [13, 41] governs the decay of the square pattern below $T_g$, in accordance with recent experimental studies[6, 9, 11, 13, 23]. The flattening of profile patterns at the free surface of films below $T_g$ has been ascribed to surface diffusion as suggested by Mullin's theory[19]. It must be noted that, since the mobile layer can still be considered at equilibrium within a certain temperature range below $T_g$, and thus the Stokes-Einstein relation is valid there, one can also describe the surface mobility as a surface flow which leads to an identical partial differential equation for the profile's evolution[9]. Surface diffusion levels a sinusoidal surface pattern at a decay rate proportional to $q^4$, where $q$ is the angular wavenumber. Other mechanisms, such as bulk viscous flow and evaporation-condensation exhibit weaker $q$ dependences (except for the limiting lubrication case, that accidently shows[9] the same $q^4$ dependence for a bulk viscous flow above $T_g$). We have not investigated the angular wavenumber dependence of the decay rate below $T_g$ here but, instead, we have carried out a layer-resolved analysis of the more abundant A type particles' $z$-dependent mean-squared displacements (MSDs) as defined by:

$$\Delta \boldsymbol{r}^2(z,t) \;=\; \left\langle \frac{1}{n_t} \sum_i |\boldsymbol{r}_i(t) - \boldsymbol{r}_i(0)|^2 \right\rangle . \qquad (3)$$

Here $\boldsymbol{r}_i(t)$ is the position of particle $i$ at time $t$ and $\langle \ldots \rangle$ is an ensemble average. This definition takes into account only the $n_t$ particles which are at all times $t' < t$ within the slab centred at $z$ and bearing a width of $\Delta z \;=\; 1.5$. The results for the runs carried out at $T$ = 0.35 are presented in Fig.5. For comparison purposes, the results for runs carried out above $T_g$, at $T$ = 0.46, are also shown. The simulation runs at $T$ = 0.46 were significantly shorter than the runs below $T_g$ due to major evaporation of the surface particles.

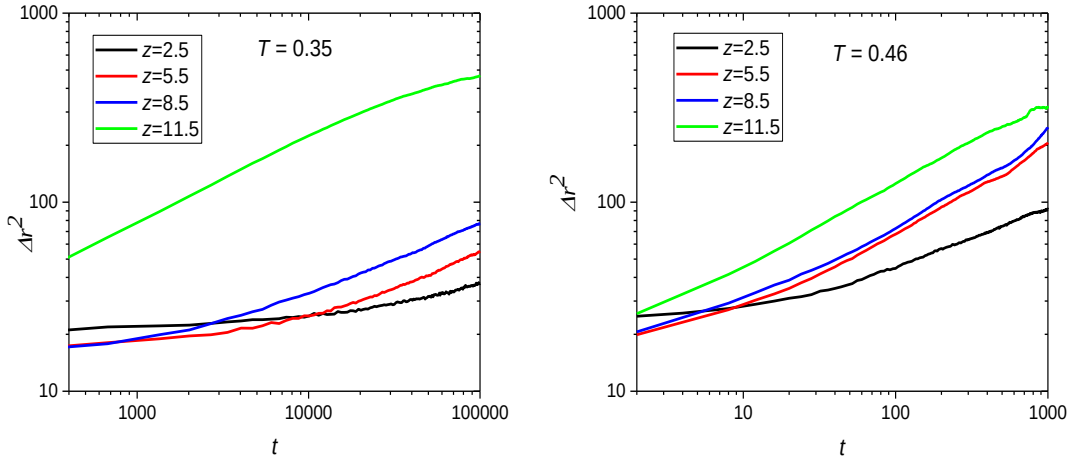


Figure 5: Layer-resolved mean-squared displacements (see eq.3), for various distances $z$ from the substrate as indicated, at temperature $T$ = 0.35 (left) and $T$ = 0.46 (right).

Focusing on the left panel of Fig.5, it appears that, at $T$ = 0.35, the MSD of the particles located in the outermost film layer near the film surface is about 5 times larger than the one for the particles in the second outermost film layer. There is no sign of major propagation of the enhanced surface mobility into the bulk in contrast to the case above $T_g$, as shown on the right panel. This observation corroborates a scenario in which the relaxation of the square pattern is governed by surface diffusion below the glass transition. A similar behaviour was observed at all sampled temperatures below $T_g$.

Finally, the diffusion coefficients $D_s$ for the surface particles were extracted from the MSD curves (see Fig.5) for different temperatures, and are compared with the corresponding bulk values $D_b$ in Fig.6.

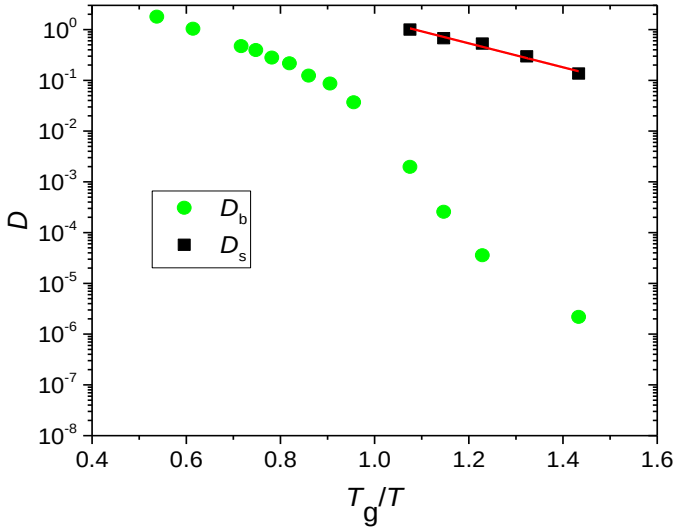


Figure 6: Diffusion coefficients for the top-layer ($D_s$) and bulk ($D_b$) particles versus inverse temperature. The latter is scaled by the bulk $T_g$. The solid line is an affine fit in log-linear representation.

As it can be discerned, the diffusion coefficients of the surface particles seem to exhibit an Arrhenius-type temperature dependence, which is reminiscent of previous observations for oligomer glasses [6, 9]. Diffusion at the surface is faster than in the bulk by a factor that ranges from $10^2$ to $10^4$ at the lowest temperatures studied. This ratio drastically rises with cooling as it has been observed in both experimental and theoretical studies[6, 9, 13, 40].

## IV. Conclusions

Molecular dynamics simulations have been conducted in order to examine the decay process of a periodic square-wave pattern at the free surface of a binary Lennard-Jones liquid. Contrary to previous simulation studies, the evolution of the height was examined over a wide temperature range sampling both the liquid and glassy states of the film. Different mechanisms appeared to control the relaxation at these two states. By the aid of layer-resolved analysis of the particles' mean-squared displacements, we show that diffusion is much more efficient in the layer close to the free surface than elsewhere in the bulk. Specifically, the diffusion coefficient of the surface particles reaches a value $10^4$ times larger compared to the one for the particles in the bulk and this difference grows upon cooling.

**Acknowledgements**

The authors gratefully acknowledge financial support from ANR WAFPI and ANR FSCF, as well as the Global Station for Soft Matter, a project of Global Institution for Collaborative Research and Education at Hokkaido University. Hendrik Meyer is kindly thanked for providing the layer-resolved analysis code. The authors also thank Anthony Maggs, Elie Raphaël, Kari Dalnoki-Veress, James Forrest, Joshua McGraw Oliver Bäumchen and Jörg Baschnagel for stimulating discussions. K.K would like to thank FO.R.TH.-IESL for the warm hospitality during his stay there.

**References**

1. M. Ulbricht, Polymer 47, 2217 (2006).
2. M. Hasebe, D. Musumeci, C. T. Powell, T. Cai, E. Gunn, L. Zhu, and L. Yu, J. Phys. Chem. B 118, 7638 (2014).
3. Y. Sun, L. Zhu, K. L. Kearns, M. D. Ediger, and L. Yu, Proc. Natl. Acad. Sci. U.S.A. 108, 5990 (2011).
4. M. D. Ediger, Proc. Natl. Acad. Sci. U.S.A. 111, 11232 (2014).
5. J. H. Mangalara, M. D. Marvin, and D. S. Simmons, J. Phys. Chem. B 120, 4861 (2016).
6. Z. Yang, Y. Fujii, F. K. Lee, C.-H. Lam, and O. K. C. Tsui, Science 328, 1676 (2010).
7. Z. Yang, A. Clough, C.-H. Lam, and O. K. C. Tsui, Macromolecules 44, 8294 (2011).
8. M. K. Mapes, S. F. Swallen, and M. D. Ediger, J. Phys. Chem. B 110, 507 (2006).
9. Y. Chai, T. Salez, J. D. McGraw, M. Benzaquen, K. Dalnoki-Veress, E. Raphaël, and J. A. Forrest, Science 343, 994 (2014).
10. J. Teisseire, A. Revaux, M. Foresti, and E. Barthel, Appl. Phys. Lett. 98, 013106 (2011).
11. Z. Fakhraai, and J. A. Forrest, Science 319, 600 (2008).
12. W. Zhang, and L. Yu, Macromolecules 49, 731 (2016).
13. C. W. Brian, and L. Yu, J. Phys. Chem. A 117, 13303 (2013).
14. M. Hamdorf, and D. Johannsmann, J. Chem. Phys. 112, 4262 (2000).

15. W. Zhang, C. W. Brian, and L. Yu, J. Phys. Chem. B 119, 5071 (2015).
16. S. Ruan, D. Musumeci, W. Zhang, A. Gujral, M. D. Ediger, and L. Yu, J. Chem. Phys. 146, 203324 (2017).
17. H. Kim, A. Rühm, L. B. Lurio, J. K. Basu, J. Lal, D. Lumma, S. G. J. Mochrie, and S. K. Sinha, Phys. Rev. Lett. 90, 068302 (2003).
18. L. Wang, A. J. G. Ellison, and D. G. Ast, J. Appl. Phys. 101, 023530 (2007).
19. W. W. Mullins, J. Appl. Phys. 30, 77 (1959).
20. H. P. Bonzel, and E. E. Latta, Surf. Sci. 76, 275 (1978).
21. M. E. Keeffe, C. C. Umbach, and J. M. Blakely, J. Phys. Chem. Solids 55, 965 (1994).
22. L. Zhu, C. W. Brian, S. F. Swallen, P. T. Straus, M. D. Ediger, and L. Yu, Phys. Rev. Lett. 106, 256103 (2011).
23. Y. Chen, W. Zhang, and L. Yu, J. Phys. Chem. B 120, 8007 (2016).
24. C. Donati, S. C. Glotzer, P. H. Poole, W. Kob, and S. J. Plimpton, Phys. Rev. E 60, 3107 (1999).
25. W. Kob, C. Donati, S. J. Plimpton, P. H. Poole, and S. C. Glotzer, Phys. Rev. Lett. 79, 2827 (1997).
26. H. C. Andersen, Proc. Natl. Acad. Sci. U.S.A. 102, 6686 (2005).
27. W. Kob, J. Phys. Condens. Matter 11, R85 (1999).
28. P. Scheidler, W. Kob, K. Binder, and G. Parisi, Philos. Mag. B 82, 283 (2002).
29. G. M. Hocky, L. Berthier, W. Kob, and D. R. Reichman, Phys. Rev. E 89, 052311 (2014).
30. P. Scheidler, W. Kob, and K. Binder, EPL Europhys. Lett. 59, 701 (2002).
31. F. Varnik, P. Scheidler, J. Baschnagel, W. Kob, and K. Binder, Mater. Res. Soc. Symp. Proc. 651, T3.1.1 (2000).
32. P. Scheidler, W. Kob, and K. Binder, EPL Europhys. Lett. 52, 277 (2000).
33. P. Scheidler, W. Kob, and K. Binder, J. Phys. Chem. B 108, 6673 (2004).
34. S. Singh, M. D. Ediger, and J. J. de Pablo, Nat. Mater. 12, 139 (2013).
35. P.-H. Lin, I. Lyubimov, L. Yu, M. D. Ediger, and J. J. de Pablo, J. Chem. Phys. 140, 204504 (2014).
36. F. C. Marcos, and V. A. Ezequiel, J. Phys. Condens. Matter 21, 263001 (2009).
37. K. Kayhani, K. Mirabbaszadeh, P. Nayebi, and A. Mohandesi, Appl. Surf. Sci. 256, 6982 (2010).
38. V. V. Hoang, and T. Q. Dong, Phys. Rev. B 84, 174204 (2011).

39. A. Haji-Akbari, and P. G. Debenedetti, J. Chem. Phys. 141, 024506 (2014).
40. R. Malshe, M. D. Ediger, L. Yu, and J. J. de Pablo, J. Chem. Phys. 134, 194704 (2011).
41. I. Tanis, H. Meyer, T. Salez, E. Raphaël, A. C. Maggs, and J. Baschnagel, J. Chem. Phys. 146, 203327 (2017).
42. W. Kob, and H. C. Andersen, Transport Theor. Stat. Phys. 24, 1179 (1995).
43. W. Kob, and J.-L. Barrat, Phys. Rev. Lett. 78, 4581 (1997).
44. R. Li, L. Wang, Q. Yue, H. Li, S. Xu, and J. Liu, New J. Chem. 38, 683 (2014).
45. W. Smith, and I. T. Todorov, Mol. Simul. 32, 935 (2006).
46. T. G. A. Youngs, J. Comput. Chem. 31, 639 (2009).
47. S. S. Ashwin, and S. Srikanth, J. Phys. Condens. Matter 15, S1253 (2003).
48. Y. Sano, K. Nishio, J. Kōga, T. Yamaguchi, and F. Yonezawa, J. Non-Cryst. Solids 345-346, 546 (2004).